Downscaling wind and wavefields for 21st century coastal flood hazard projections in a region of complex terrain

A. C. O'Neill[1] (ID), L. H. Erikson[1] (ID), and P. L. Barnard[1] (ID)

[1]Pacific Coastal and Marine Science Center, United States Geological Survey, Santa Cruz, California, USA

Abstract While global climate models (GCMs) provide useful projections of near-surface wind vectors into the 21st century, resolution is not sufficient enough for use in regional wave modeling. Statistically downscaled GCM projections from Multivariate Adaptive Constructed Analogues provide daily averaged near-surface winds at an appropriate spatial resolution for wave modeling within the orographically complex region of San Francisco Bay, but greater resolution in time is needed to capture the peak of storm events. Short-duration high wind speeds, on the order of hours, are usually excluded in statistically downscaled climate models and are of key importance in wave and subsequent coastal flood modeling. Here we present a temporal downscaling approach, similar to constructed analogues, for near-surface winds suitable for use in local wave models and evaluate changes in wind and wave conditions for the 21st century. Reconstructed hindcast winds (1975–2004) recreate important extreme wind values within San Francisco Bay. A computationally efficient method for simulating wave heights over long time periods was used to screen for extreme events. Wave hindcasts show resultant maximum wave heights of 2.2 m possible within the Bay. Changes in extreme over-water wind speeds suggest contrasting trends within the different regions of San Francisco Bay, but 21th century projections show little change in the overall magnitude of extreme winds and locally generated waves

Plain Language Summary Near-surface winds are temporally downscaled for use in historical and 21st century wave models. Extreme wave height events are identified using an efficient simulation method for long time periods. Potential changes in 21st century extreme wind and wave conditions are evaluated.

1. Introduction

Coastal flooding is a significant risk to communities worldwide and will pose increasing risk in many areas as predominant contributions to flooding, including storms and sea level, are altered with climate change. With millions of people residing in low-lying regions vulnerable to coastal flooding [*Nicholls*, 2004], conservative projections of ~1 m sea level rise (SLR) [*Vermeer and Rahmstorf*, 2009; *National Research Council*, 2012] could cost up to $1 trillion in evacuating inundated communities, in addition to infrastructure and urban damage. Surge and waves from storms can further exacerbate coastal flood hazards, raising water levels an additional 2 m or more [*Guza and Thornton*, 1981; *Allan et al.*, 2011]. Coastal and estuarine resource managers and local governments therefore look to science to provide insight into how climate change, including storm changes and resulting waves, may affect their areas. One such science-based tool is the Coastal Storm Modeling System (CoSMoS) [*Barnard et al.*, 2014], which provides numerically derived coastal flooding predictions due to both sea level rise and storms affected by climate change. CoSMoS was recently implemented within San Francisco Bay, CA (USA), as an extension of work focused on the open Pacific coast. CoSMoS includes storm and wind changes for the 21st century through use of global climate models (GCMs). The wave climate within the interior of the Bay, largely sheltered from the outer coast, is dominated by local wind-generated waves rather than long-period swell. While the height of wind waves within this fetch-limited environment may not be as great as on the outer coast, contribution to coastal flooding is not trivial as waves can enhance flooding associated with storm surge or other atmospheric-driven increases in water levels [*Ryan et al.*, 1999; *Conner et al.*, 2011] along the low-lying estuarine shoreline. In this location, native GCM near-surface winds are too coarse and not appropriate for use in this topographically complex region, where high spatial and temporal resolution winds are critical for capturing regional trends and mesoscale variability driving locally generated wind waves.

Historical wind observations and constructions may offer the temporal resolution needed for hindcast studies. *Kerper et al.* [2011] used historical wind constructions to model waves in the Bay, but the wind

fields lack the observed spatial variation, which may greatly affect the spatial distribution and height of modeled waves. Additional wind field constructions are available for short periods or durations of study [*Ludwig et al.*, 1991] but are not sufficient for a complete climatological analysis (~30 years). Most importantly, constructions based on historical observations may not represent future conditions, specifically the character or frequency of extreme events in the 21st century. *Cloern et al.* [2011] showed that the occurrence of extreme sea levels within the Bay are likely to increase in the 21st century and that extreme sea level anomalies related to storms in this region are associated with higher wave heights [*Cayan et al.*, 2008]. Additionally, *Erikson et al.* [2015] showed that while open-ocean extreme wave heights are projected to decrease along much of the California coast, likely as a result of changing North Pacific storm-generation areas, the direction of projected extreme wave events are likely to be more southerly. Such changes in frequency, intensity, and direction may result in future extreme events that significantly deviate from historical analogues of high-risk events. Implementation of CoSMoS within the Bay area for 21st century risk projections therefore necessitates downscaling of GCM projections.

Numerous robust GCM-downscaling projects have been conducted for North America, but many of these primarily focus on temperature and precipitation for hydrologic modeling [*Maurer et al.*, 2007; *Hidalgo et al.*, 2008; *Brekke et al.*, 2013; *Pacific Climate Impacts Consortium*, 2014] and do not include wind outputs. Some dynamical downscaling projects offer wind projections but only for limited decadal periods [*Hall et al.*, 2012]. Out of the numerous statistical and dynamical downscaling projects available or in progress for the North American region, Multivariate Adaptive Constructed Analogues (MACA) [*Abatzoglou and Brown*, 2012] has high spatial resolution GCM wind projections over the Bay area for the entire 21st century. MACA is a statistically downscaled model available for the western U.S., derived from a selection of Coupled Model Intercomparison Project Phase 5 (CMIP5) GCMs [*Taylor et al.*, 2012]. MACA is similar in construction to other Constructed Analogues (CA) [*Hidalgo et al.*, 2008] but uses an observational data set to remove historical bias and fit appropriate spatial patterns in the output. Having near-surface zonal/meridional wind (*u/v*) available at a resolution of 4 km, MACA data sets are spatially more representative of SF Bay conditions than GCMs. For instance, only a single grid point from the Geophysical Fluid Dynamics Laboratory's (GFDL) Earth System Model ESM-2M [*Dunne et al.*, 2012] represents conditions for the entire Bay area. Comparisons with historical data (section 2 of this paper) show best agreement to observations at San Francisco International Airport, but with significant bias, especially in extreme values, in specific regions. Wind fields generated with MACA more accurately depict conditions in the numerous microclimates across the Bay. However, like other similar statistically downscaled products, MACA only provides a representation of projected values on a daily timescale that does not resolve peak wind forcing during extreme events, critical to fully evaluating the potential for coastal flooding and damage. Therefore, further work is required to achieve temporal resolution with MACA data sets to adequately model San Francisco Bay wind waves during storms.

Here we present a temporal downscaling approach for near-surface winds suitable for use in local wave models. The downscaled high-resolution wind fields were subsequently used as boundary conditions in a numerical model to simulate waves within the Bay for hindcast and 21st century periods. The input data and resulting time series were used to address two objectives: (1) assess the need and ability of the temporal downscaling technique to adequately represent extreme wind waves in the fetch-limited waters of San Francisco Bay and (2) evaluate potential changes in extreme wind and wave conditions for the 21st century. By comparing time-downscaled historical extreme wind reconstructions to observations, we can assess how well the methodology recreates potentially significant extreme wind speed variation. Spatial wavefields simulated for the historical and 21st century time periods using the time-downscaled winds are similarly compared. While the downscaling method shows need of improvement for isolated areas, and results of the method's shortcuts underestimate contributions of wave-current interaction to wave height, the process is sufficient to identify potential trends and major storm events (requiring more complex simulation methods for further analysis) within this complex, fetch-limited region.

1.1. Study Area
1.1.1. Bay Geography
San Francisco Bay is affected by strong tidal currents, waves, and swell in the central portion immediately landward of the Golden Gate [*Barnard et al.*, 2013]. While the complete Bay area watershed and coastal system encompasses expansive areas of the neighboring Pacific coast and the Sacramento-San Joaquin Delta,
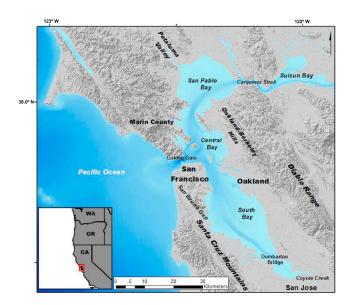
Figure 1. San Francisco Bay study area with wind-wave generation basins of interest: Suisun Bay, San Pablo Bay, Central Bay, and South Bay.

this study is focused on the contiguous estuarine waters of the Bay interior consisting of four regions (Figure 1): South Bay, Central Bay, San Pablo Bay, and Suisun Bay (the latter two referred to as North Bay).

Much of San Francisco Bay is bordered by numerous levees, residential and urban areas, tidal marshes, and wetland restoration projects. Multiple rows, or layers, of leveed salt ponds are prevalent in the far south and eastern edge of the South Bay. The ponds interrupt surface propagation and block wave energy from the Bay to the shore. Fetch narrows at the Dumbarton Bridge, severely limiting wave propagation and generation to the farthest southern reaches of this region.

Central Bay is the deepest part of the Bay, averaging over 25 m deep in the western portion [*Barnard and Kvitek*, 2010], and is affected by open ocean swell propagating through the mouth at the Golden Gate [*Talke and Stacey*, 2003], which reaches depths of 113 m [*Barnard et al.*, 2006].

The North Bay region has significant expanses of wetland near the mouths of Sonoma Creek, and the Petaluma and Napa Rivers, as well as complex networks of ponds and levees in the northern reaches of San Pablo Bay (Figure 1) interrupting wave propagation to shore. Suisun Bay is an extremely shallow basin protected by an intricate system of levees and dikes. Occasional channels 10–15 m deep run between managed marsh areas and connect to the primary channel, but the bulk of Suisun Bay is much shallower, less than 5 m deep [*Ganju et al.*, 2011]. Beyond the low-lying marsh areas, Suisun Bay is bounded by higher terrain (>150 m) to the west and south.

1.1.2. Winds

San Francisco Bay displays seasonal patterns and mesoscale trends governed by changes in synoptic-scale forcing. Numerous mountain ranges, hills, valleys (see Figure 1), and separated bays can drastically affect the near-surface wind behavior, creating varied regional conditions with respect to wind direction or speed [*Patton*, 1956]. While the greatest regionalized distinctions occur in lighter wind conditions [*Ross*, 2001], such as in summertime and in between wintertime storms, variation in direction and magnitude of strong wind events can significantly affect wave generation in the different regions of the Bay area. As the objective of this study is identifying extreme wind-wave events, focus will be on wintertime storm events.

Wintertime storm events drive most of the highest observed winds and waves in the Bay [*National Climatic Data Center (NCDC)*, 2013; *National Oceanic and Atmospheric Administration (NOAA)*, 2016a] and the most variable Bay-wide wind directions [*Ross*, 2001]. While Bay-wide storm wind conditions reflect transiting storms rather than strong microclimate signatures as shown in summer [*Ross*, 2001], periods in between winter-transiting storms are often characterized by calm, low-speed wind conditions. Storm systems can bring high-wind conditions throughout the region, occasionally severe enough to exceed storm force criteria (24.6 m/s). The highest official recorded over-water or near-water wind speeds are in Central Bay, peaking at 34 m/s [*NOAA*, 2016a]. The stronger winds in this region are due to amplification through the Golden Gate and along Bay-axis and little topographic sheltering from open-ocean storm winds. Another region of topographically amplified winds is within Carquinez Straight between the northern San Pablo and Suisun Bays [*Patton*, 1956; *Ross*, 2001]. Extreme winds are lowest in South Bay, compared to observed maxima in Central or North Bays [*NCDC*, 2013; *NOAA*, 2016a].

A weather-pattern analysis of San Francisco Bay [*Ross*, 2001] suggests that the strongest winter winds have a southerly component. Coastal studies outside the Bay reinforce this [*Dorman and Winant*, 1995], showing the

strongest winter winds from the south, typically preceding a low pressure system, or from the north just following a low pressure system's frontal passage, with both categories showing predominantly alongshore (northwest-southeast) directionality. Observations [*NCDC*, 2013; *NOAA*, 2016a] show that highest wind speeds occur at subdaily timescales along the Bay's coastline. Depending on specific storm and wind direction, some Bay regions are also influenced by orographic effects, creating areas of enhanced or reduced wind speed.

1.1.3. Waves

Given the complex surrounding terrain and semi-isolated subregions of the Bay, the area is a fetch-limited environment, and local, wind-generated waves are dominant with the exception of Central Bay [*Talke and Stacey*, 2003; *Hanes et al.*, 2011] . Quantitative information in regards to a spatially expansive historical wave climate for the Bay is limited, and much of what is known about wave conditions is based on limited-duration field data [*Putnam*, 1947; *Talke and Stacey*, 2003; *Lacy and Hoover*, 2011; *Lacy et al.*, 2014], shoreside observations during storm events [*Ryan et al.*, 1999; *NOAA*, 2016a], and professional anecdotal evidence from the maritime industry (*Marine Exchange of the San Francisco Bay Region*, 2016). The largest reported waves are associated with wintertime storms, with the highest waves reported in southern San Pablo and Central Bays. As mentioned, Central Bay also receives swell from the open ocean transiting through Golden Gate. Shore-based reports have described waves of ~2 m near urban shore areas in the central portion of the Bay [*Ryan et al.*, 1999]. Sensitivity studies by *van Raalten et al.* [2009] have shown possible maximum significant wind-wave heights (H_s) of just over 2 m within the central to northern portions of the Bay due to extreme winds (>20 m/s), consistent with both shoreside and maritime observations.

2. Data and Methods

2.1. Observation Records

Long-term records of four key observation stations within the Bay were used in this study: San Francisco International Airport (SFO), Oakland International Airport (OAK), San Jose International Airport (SJC), and Travis Air Force Base (TRAV) (Figure 2). These stations have lengthy historical records with high quality and limited data gaps. They are also broadly representative of over-water conditions (with SFO and OAK immediately bordering the Bay shoreline) within the Bay and illustrate similar changes in weather and general climatology [*Kerper et al.*, 2011]. Data at these four stations were subsampled into two 30 year libraries for use in downscaling: (1) daily average and (2) 3-hourly vector components (u/v).

While maximum wind speeds are recorded for several shoreside stations within the regions of interest, little exists in terms of long-term records for over-water extreme wind speeds; wind remains unhindered by higher topographic friction observed over land, and funneling and terrain may enhance near-surface wind speeds. To estimate the possible extremes of over-water wind speeds, NOAA's National Climatic Data Center (NCDC) storm event database [*National Climatic Data Center (NCDC)*, 2013] was scoured for high wind events affecting the Bay area since the start of the database in 1998. From this database, a record of maximum sustained wind speeds was collated for locations immediately adjacent to the Bay or of likely similar overwater conditions. Gusts were not included, as sustained winds are necessary to building waves of interest. In cases where only gust observations were available, a wind gust ratio of 1.3 was used to adjust values to sustained wind speeds, well within operational ranges of sustained-gust ratios [*Joyner*, 2013; *Solari*, 1993]. This maximum sustained wind speed record served as benchmarks of probable maximum wind speed projections in each subregion, 40 m/s and 30 m/s in North/Central and South Bays, respectively.

2.2. Climate Model

MACA data sets are available for several CMIP5 21st century scenario projections (Representative Concentration Pathway (RCP) 4.5 and 8.5 for 2010–2100) and hindcasts (1950–2004) and are based on numerous parent GCMs [*Abatzoglou and Brown*, 2012]. MACA downscales parent GCMs to 4 km resolution gridded data by identifying analogues in high-spatial-resolution meteorological data sets obtained from a variety of sources including reanalysis outputs, model data, and weather-network observation stations [*Abatzoglou*, 2013]. Near-surface (10 m height) zonal/meridional winds, temperature, precipitation, humidity, and surface downward shortwave radiation are downscaled at a daily time step, representative of the daily average. GCM outputs are bias-corrected in the MACA process, before and after identification of analogues. Additionally, MACA accounts for projections which lack appropriate analogues and improves upon
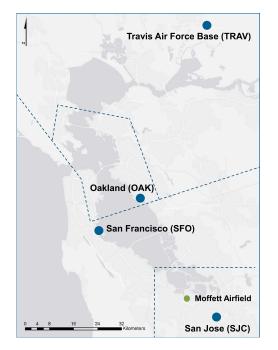
Figure 2. Key observation stations used in temporal downscaling and respective Bay area subregions: Travis Air Force Base (TRAV) for North Bay (San Pablo Bay and Suisun Bay), Oakland International Airport (OAK) for Central Bay, San Francisco International Airport (SFO) for the greater part of South Bay, and San Jose International Airport (SJC) and Moffett Airfield (used to modify SJC) for the furthest southern portions of the Bay.

traditional CA techniques by incorporating additional steps to preserve trends in specific variables (e.g., temperature and precipitation). MACA wind projections have good skill compared to other statistically downscaled data sets; however, it is noted that extreme wind speeds (upper quantiles) are characterized better than low wind speeds [*Abatzoglou and Brown*, 2012].

For this study, MACA data derived from GFDL ESM2M were used (data set hereafter referred to as MACA-GFDL). GFDL was chosen to be consistent with previous outer-coast model implementations, allowing for temporal synching of results between inside and outside the Bay, and previous work has shown that GFDL ESM2M wind and derived wavefields roughly represent the median range of GCMs in terms of wind and sea level pressure forcing in the Eastern Pacific [*Erikson et al.*, 2015]. Historical (MACA data sets based from GFDL ESMS2M output

for 1950–2005) and RCP 4.5 10 m height zonal/meridional wind projections were employed in generating Bay area wind fields for wave generation. Observations show MACA-GFDL spatially downscaled over the historical period to be broadly representative of mean daily conditions Bay-wide but shows regional variability in similarity (see Figure 3). Paying particular attention to the extreme vector component values (upper quantiles), MACA-GFDL shows negative bias at SFO and TRAV, under-representing observed extremes of daily average vector components, while extremes at OAK are overpredicted in MACA-GFDL. Extremes at SJC, which shows the weakest representation by MACA-GFDL (Figure 3), are up to 4 m/s lower than depicted in MACA-GFDL. To consider the extent of this variation in similarity due to climatic variation, observations were split into two periods (1975–1989 and 1990–2004) and compared using the Kolmogorov-Smirnov test. Bay-wide (average of all stations) comparisons show that MACA-GFDL simulates meridional components best, with model-observation variation ($d = 0.14$) on the order of natural climatic variability ($d = 0.13$). Zonal components of MACA-GFDL show more discrepancy, as Bay-wide model-observations comparisons ($d = 0.19$) differ more than natural variability ($d = 0.08$).

2.3. Wind Downscaling Method

In order to provide higher temporal resolution than available in MACA-GFDL data sets, a concept similar to the constructed analogue was applied in the time domain. Instead of a obtaining a spatial analogue, depicting high-resolution wind patterns over an area, a "best match" day from a 30 year library of observations from the four key stations around the Bay (SFO, OAK, SJC, and TRAV) was identified and used to "fill-in" the daily variation lacking in the MACA-GFDL data sets.

The study area was first split into four separate subregions, each containing a high-quality observation station with a robust record and broadly representative of distinct subregional climatologies. This regionalization is framed off of work conducted by *Kerper et al.* [2011], where only three general observation stations were used to characterize variation in historical Bay-area wind conditions, roughly segmented into North, Central, and South Bays. However, while wind speed distributions for much of South Bay are similar to distributions at SFO, the far southern portions of the Bay display extreme wind values up to 5 m/s lower than observed
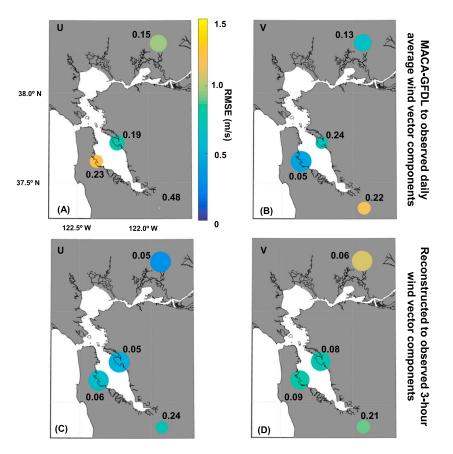
Figure 3. Comparisons of vector wind component ECDFs for key observations stations (1975–2004), where distribution similarity (size of dot) is determined by Kolmogorv-Smirnov test (d, also listed next to station) and distribution RMSE is shown by color shading. Comparisons are shown for (a and b) daily average vector components of originating MACA-GFDL to observations and (c and d) 3-hourly vector components of time-downscaled reconstructed data to observations.

elsewhere in the Bay. Therefore, this region was recognized as a distinct subregion, represented by winds at SJC (Figure 2).

Before performing temporal downscaling on a MACA-GFDL wind field, site-specific quantile corrections were applied to the key station locations (SFO, OAK, SJC, and TRAV) at each projected daily time step (τ). The empirical cumulative distribution function (ECDF) from each key station's 30 year daily average vector component observational wind record was compared to MACA-GFDL wind data for the same location and historical period to obtain a site-specific quantile correction (in both u and v). This arithmetic quantile-correction was applied for hindcast and projection data, thus preserving the correction to the distribution profiles in 21st century projections. It is noted that this method does not account for future changes in daily average distributions but instead assumes that the quantile-corrections represent adjustments to wind patterns not fully captured in the spatially downscaled model.

After correcting MACA data for bias, a "best day" match day was identified by comparing the spatial variability and fit to the library of daily average winds among all the stations for a comparable time of year, similar to CA methods [*Hidalgo et al.*, 2008]. This identification was completed by using least squares error (LSE) analysis, where the LSE was calculated for all four stations' daily u/v to MACA-GFDL's quantile-corrected vector components (equation (1)). Bay-wide error using a given analogue day (ι) from the library is

$$\varepsilon_\tau = \sqrt{\sum_i^{\text{station}} \left(\frac{\left(\text{uMG}i\tau - \overline{\text{ulib}i\iota}\right)^2}{\sigma_{\text{ulib}i\iota}} + \frac{\left(\text{vMG}i\tau - \overline{\text{vlib}i\iota}\right)^2}{\sigma_{\text{vlib}i\iota}} \right)} \qquad (1)$$

where uMG$i\tau$ is the zonal vector component (u) of MACA-GFDL for station i on projection day τ, $\overline{\text{ulib}i\iota}$ is the

daily average library analogue u for the same station, v is the meridional vector component for the same, and σ_{ulib} and σ_{vlib} are the variance of the library zonal and meridional components, respectively. The best match analogue ι was identified as having the least error:

$$\min_{\iota} \varepsilon_{\tau_{\iota}}$$

LSE were only calculated for days ι within a 40 day, subseasonal window of the MACA-GFDL wind field being downscaled or within 20 days preceding and following τ's year day. For example, if τ was on 1 November 2050, the 30 year library of all days between 11 October ($\tau - 20$ days) and 21 November ($\tau + 20$ days) was searched for the best spatial match. By keeping the comparisons within a relatively small window relative to time of year, seasonal variations are preserved and erroneous matches (e.g., using a summertime vector component profile for a wintertime scenario) are avoided.

Once a best match was identified from the daily average library, Δu (Δv) between uMGτ (vMGτ) and $\overline{\text{ulib}\iota}$ ($\overline{\text{vlib}\iota}$) was calculated for each station. These match offsets were converted to a speed ratio correction ($\overline{S}_{libi}/S_{\text{MACA-GFDL}}$) and directional offset ($\pm$degrees). Corrections were made to speed and direction, rather than u/v, as results were more stable when corrections crossed cardinal directions (e.g., north, south, east, or west). This offset was applied to all MACA-GFDL grid points within each station's subregion to account for disparities between the identified time analogue and projected u/v. At this stage, daily variation could be incorporated with the projection day's average u/v. Within each station's subregion, station-specific u/v 3-hourly variation (daily average removed) for the best match day (ι) was applied to the quantile-corrected and spatially varying MACA-GFDL wind field, thus expanding MACA-GFDL daily u/v data at a projection day τ to u/v data at $\tau(0\,h)$, $\tau(3\,h)$, … $\tau(21\,h)$. Grid points along the subregion borders were spatially interpolated between the subregions at each 3 h time step to reduce discontinuities within the wind field. In this way, the high-resolution spatial variation provided by MACA-GFDL is maintained, and it is overlaid with daily wind variation, characterized by the subregion's station.

The method was slightly modified for South Bay. In researching possible observations stations and proxies for this region, Moffett Field in Mountain View (MTN) was a preferred choice because of its location immediately adjacent to the Bay. However, large data gaps in the historical record made the station unsuitable to use. The record length for good, continuous data available for MTN is only 10 years, so SJC's 30 year record was used instead for the southernmost reaches of the Bay. Distribution profiles between MTN and SJC are very similar and differ significantly only in the extremes. Extreme values in both vector components were up to 10 m/s higher at SJC than MTN (not shown). Therefore, to ensure the best possible match for over-water conditions, SJC's observations were quantile-corrected (ECDF to ECDF as above) to MTN's distribution once a match was made. The correction was calculated from a coincident time series (1975–1984) for MTN and SJC and was used to create profiles in the far South Bay that more accurately reflect conditions represented at the area.

2.4. Methods for Wind-Wave Generation

The numerical wave model SWAN (Simulating Waves Nearshore), applied through the Deltares Delft3D WAVE module, was used to investigate waves generated with historical and projected time-downscaled MACA-GFDL wind fields. SWAN is a third-generation spectral wave model capable of simulating wind-wave growth, propagation, refraction, dissipation, and depth-induced breaking [*Ris*, 1997; *Booij et al.*, 1999].

Using a single, curvilinear grid encompassing all Bay subregions (Figure 4a), wind-generated waves were modeled for the entire 21st century. To optimize both model efficiency and resolve wave generation processes, resolution on the grid varied from ~400 m × 400 m in the subregion interiors to approximately 50 m × 50 m near shore and in significantly terrain-affected areas (i.e., areas of likely funneling). Model depth values were constructed from a 2 m resolution digital elevation mode (DEM), utilizing the latest lidar, multi-beam, and single-beam sonar data sets [*Tyler et al.*, 2014]. Grid point depth values were calculated as an average from the four closest DEM samples. Wave frequencies were lognormally distributed into 37 bins ranging from 0.03 Hz to 1 Hz and with 10° direction bins. Depth-induced breaking was computed with the *Battjes and Janssen* [1978] formulation (with a breaking index of 0.73), while whitecapping was described with the *van der Westhuysen et al.* [2007] expression. Bottom friction was based on the Joint North Sea Wave Project formulation with the friction coefficient set for local seas at 0.067 m^2/s [*Hasselmann et al.*, 1973].
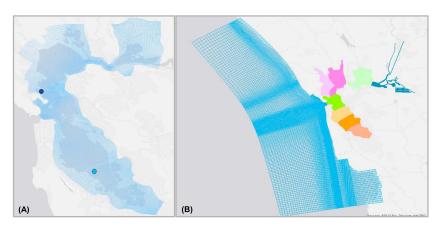
Figure 4. Model grids employed in San Francisco Bay. (a) SWAN model grid for simulation of waves. Wave observation locations are shown with circles in South Bay (light blue) and Corte Madera (dark blue). (b) Delft3D-FLOW model grid for simulation of tides and currents. FLOW model consists of nine coupled grids.

For evaluation of wave-model skill (section 3.2.1), the effects of SLR (section 3.2.3), and sensitivity testing (see the supporting information), the SWAN model was coupled with a previously calibrated Delft3D circulation model [*Elias and Hansen*, 2012; *Erikson et al.*, 2013], extending into the Pacific Basic to accurately account for tidal exchange through the Golden Gate (see the supporting information). These simulations are run over multiple tidal cycles to capture the effects of water-level changes, tidal impacts, and wave-current interaction.

A straight-forward approach for determining wave heights for the 21st Century period would be a fully coupled flow-wave simulation for the entire period using the projected winds. However, such a model setup is computationally prohibitive. In the interest of reducing computation time while only seeking a characterization of extreme conditions for the 21st century projection period, two critical assumptions are made: (1) the wave-model time step can be increased (from 3-hourly wind output) such that a fully developed sea-state is still captured, and (2) the wave model can be computationally simplified to characterize the bulk of the extreme wave energy. These two assumptions are explored in-depth in the supporting information. Based on the sensitivity analyses for these assumptions, the wave model time step was increased from 3 h to 24 h, run in stationary mode assuming that steady state was reached at each time step (see the supporting information) [*Ris et al.*, 1999; *Rogers et al.*, 2007], and run without inclusion of currents (i.e., not coupled to the Delft3D flow model). With the larger wave-model time step, a subset of the temporally downscaled wind projections must be used. The absolute maximum overwater wind speed (S_{max}) for the entire area were identified within each projection day τ, and this wind field (τ N-h; depicting the wind field with the greatest Bay-wide wind speeds) was used in the SWAN model, resulting in a data set of daily maximum wave heights, hereafter referred to as wave-screening. This setup captures ~85% of the wave energy (see the supporting information) and is vastly more efficient than a typical wave-current model arrangement. However, it should be noted that this does not yield spatial depictions of wave height analogous to discrete wavefields modeled with greater temporal resolution through a full tidal cycle but rather depicts the maximum wave heights attained at each grid point from the extreme wind speeds (single N-h wind field containing maximum wind speeds observed over the projection day). As this study focuses on the maximum wave heights derived from storms, this is sufficient to our purpose. With the daily maximum wind data, the SWAN model was run for the 21st century projection time slice (2010–2100) and the hindcast period (1975–2004). Without these assumptions, wave-height simulations for the 2010–2100 period could take over 2000 h (see the supporting information), whereas the wave-screening process outlined above reduces the simulation to 1/6th that time. Additionally, as tidal impacts and wave-current interaction affect total wave height [*Olabarrieta et al.*, 2011, 2014] (see the supporting information), the simplified wave-screening method allows a specific inspection of wind waves, separate of tides and other independent factors.

Wave energy within the Bay is mainly generated by local winds, although, as stated previously, ocean swell penetrating through the Golden Gate can affect portions of Central Bay. Because the core intention of this study is to identify potential changes in extreme wind waves and identify extreme wind/wave events within the Bay, no swell were included in the wave-screening model. However, the influence of ocean swell is

accounted for with numerous follow-on storm-event simulations conducted as part of the more complex and comprehensive San Francisco Bay CoSMoS model. These simulations, covering a range of plausible SLR scenarios through 2100 (0.25 m to 2.0 m, at 0.25 m increments, and an extreme 5.0 m scenario) and storm events (derived from this study's wind and wave projections), were fully implemented after completion of the wave-screening in this study.

3. Model Hindcasts and Comparisons

3.1. Winds

To test the wind-downscaling method, the 30 year observational record is compared to a temporally downscaled reconstruction using historical MACA-GFDL data. Wind roses, depicting wind direction and speed over the entire reconstruction period, illustrate strong agreement between directionality and magnitude (see Figure 5). Reconstructions are best at SFO and OAK, whereas reconstructions at SJC show the least agreement with a bias toward more northerly winds and decreased wind speeds. Subdaily vector component extremes (uppermost quantile) are best captured at SFO with meridional component deviations within 0.5 m/s and a maximum zonal extreme deviation of 2 m/s (not shown). At TRAV, OAK, and SJC, deviations of up to 9 m/s in meridional component (v) extremes are present in particular directions (negative/positive v), with deviations otherwise of less than 1 m/s. Distribution comparisons between ECDFs of wind vector components from the reconstructed hindcast period to observations show temporally downscaled winds have greater Bay-wide similarity than originating MACA-GFDL (Figures 3c and 3d); distribution RMSE ranges from 0.31 to 0.76 m/s and 0.78 to 1.09 m/s for u and v, respectively.

Regional spatial and temporal variabilities in the reconstructions match general seasonal climatology and expected wind behavior, such as summertime direction reversals and wintertime storm periods. Higher wind speeds are seen in the downscaled data at all stations predominantly during winter periods, with occasional high westerly wind events in Central Bay during summer.

In the entire 30 year reconstruction, there are two separate time steps where reconstructed wind speeds exceed overwater benchmark values. These values are significantly higher than estimated probable extreme over-water winds, at ~45 m/s, and inspection of the resultant wind fields indicates likely numerical artifacts resulting from speed/direction corrections applied to over-represented gridded wind data. For these instances, data for the entire day (entire projection from originating MACA-GFDL τ) are disregarded in follow-on investigations and use in wave-screening.

As expected, time-downscaled wind extremes are significantly larger than extremes shown in MACA-GFDL daily average u/v. Persistent and dominant wind directions and influences are reflected in both time-downscaled and MACA-GFDL data sets: wind roses show similar patterns of directional dominance and relative strength of directional extremes. However, the large difference in the magnitude of the extremes in each data set (daily average to temporally downscaled) highlights the importance of subdaily variation on wind-wave generation.

3.2. Waves

3.2.1. Time Series Comparisons for Evaluation of Wave-Model Skill

Wave observations at two locations within the Bay, Corte Madera and South Bay, were used to evaluate skill of the wave model used in this investigation (Figure 4a and Table 1). Measurements were collected with a bottom-mounted acoustic Doppler velocimeter and an upward-looking Acoustic Doppler Current Profilers in a water depth of 2.5 m at Corte Madera and 3.4 m in South Bay, respectively [*Lacy and Hoover*, 2011; *Lacy et al.*, 2014]. Only subsections of the time series with relatively high-wave conditions and available wind reanalysis data were simulated with the model.

In order to isolate wave model skill from this study's wind-downscaling method, reanalysis winds from the California Reanalysis Downscaling at 10 km (CaRD10) database were used for two SWAN model evaluation runs. CaRD10 reanalysis winds were derived from dynamical downscaling of the National Centers for Environmental Prediction Global Forecast System model (1°, 6-hourly) [*Environmental Modeling Center*, 2003; *Kanamitsu and Kanamaru*, 2007a]. CaRD10 winds (10 km, hourly) have shown to better represent regional winds in some areas of coastal California compared to the commonly employed North American Regional Reanalysis (32 km, 3 hourly) [*Kanamitsu and Kanamaru*, 2007b]. As CaRD10 wind data resolution is at 10 km,
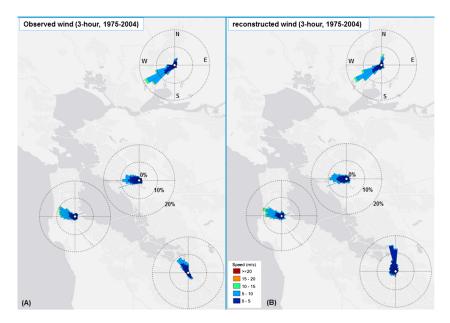
Figure 5. Wind roses of reconstructed wind data to historical records for all key subregion stations: (a) 3-hourly historical records and (b) reconstructed 3-hourly winds for 1975–2004.

some spatial variability within the Bay regions may be neglected, but this represents the best Bay-wide wind data known to the authors for an independent evaluation of the wave model skill during detailed wave-observation periods.

Maximum measured wave heights reached ~0.5 m at both sites (Table 1). CaRD10 reanalysis winds peaked at 6 m/s and 12 m/s from the southeast and east at Corte Madera and South Bay, respectively. Assuming fetch-limited but duration-unlimited winds, analytical approximations using the Shore Protection Manual [*Coastal Engineering Research Center*, 1984] nomograms suggest H_s of 0.3 m and 0.4 m at Corte Madera and South Bay, respectively, both lower than observed maximums. The numerical model better approximated H_s maximums at Corte Madera and South Bay, differing from observations by only ±0.04 m (Table 1). The numerical model overestimated mean H_s at Corte Madera versus in South Bay, but considering the rather low observed mean H_s this is not an unexpected result. The bias and root-mean-square error (RMSE) are comparable to other studies of wave dynamics in fetch limited regions (the Great Lakes with 0.04 m < bias < 0.06 m bias and 0.19 m < RMSE < 0.37 m [e.g., *Alves et al.*, 2011]).

3.2.2. Geographic Spatial Comparisons of Maximum Wave Height

In order to objectively assess the spatial variability of wave-height separate from the originating variability of wind, coupled wave-current simulations with uniform winds were completed to evaluate patterns of plausible maximum in-bay H_s and compare with observations and professional anecdotal evidence. Uniform winds, ranging in speed from 4 m/s to 24 m/s and rotated incrementally (every 1°) from 0° to 359°, were allowed to blow over the entire SWAN domain. Each wind direction and speed combination was simulated for two full days over two tide cycles to achieve fully developed fetch-limited sea states. Simulations were performed in a stationary mode, which is expected to only introduce small errors [*Ris et al.*, 1999; *Rogers et al.*, 2007] (see the supporting information).

Simulation results provide a look-up table of maximum H_s for the range of plausible wind speeds (≤24 m/s), directions, and locations within the Bay (Figure 6). Maximum H_s attained at each location was identified in

Table 1. Locations and Error Statistics of Observed and Modeled Significant Wave Heights, H_s, in North and South San Francisco Bay

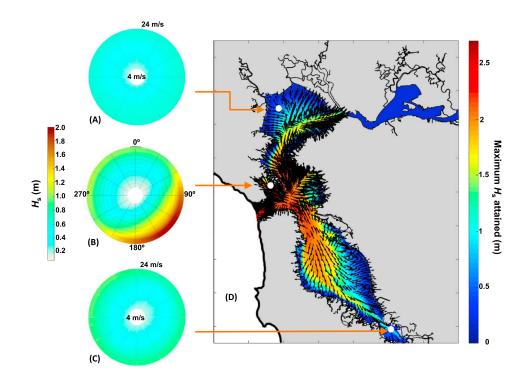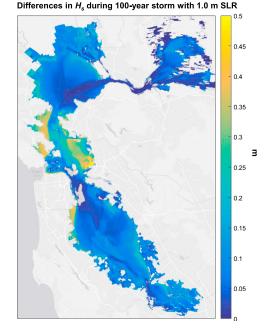| Location	Depth (m)	Time Period	Observed Mean/Max (m)	Modeled Mean/Max (m)	RMSE (m)	Bias (m)
Corte Madera (N37.92772, W122.47967)	2.5	14–25 February 2010	0.05/0.52	0.11/0.48	0.13	−0.06
South Bay (N37.58633, W122.20977)	3.4	9 September to 3 October 2009	0.09/0.50	0.12/0.54	0.08	−0.04

Figure 6. Numerically modeled maximum wave heights (H_s) throughout San Francisco Bay in response to unidirectional, constant winds. Spatially uniform, constant winds ranging in speed from 4 m/s to 24 m/s were allowed to blow over the model domain and rotated incrementally from 0° to 359°. (a–c) Maximum local wind-generated H_s as a function of wind direction (blowing from) and speed (concentric circles, with highest wind speed toward the outer edge). (d) Spatial plot of maximum Hs (color shading) attained with the 24 m/s wind speed. Incident wind directions (blowing from) that produced maximum Hs are shown with black arrows.

conjunction with its originating storm wind direction to produce a composite map of maximum H_s from storm wind speeds (24 m/s) (Figure 6). This map also helps illustrate important wind directions for wave generation. Model results show that higher maximum H_s are generated in areas with longer fetch and deeper waters of San Francisco Bay, including along the axial channels in South and North Bay and throughout most of Central Bay, where depths approach 100 m near the Golden Gate. This is consistent with observations and anecdotal evidence that report waves in excess of 2 m in this area (see section 1.1.3). In South Bay, maximum waves are generated by along-Bay axis winds from the north, except for the eastern borders of this region, where maximum waves can be driven more by westerly winds. San Pablo maximum wave heights are generated by two general directions, with northerly winds driving the largest significant waves along the southern edges of San Pablo Bay, while the majority of the subregion experiences maximum waves during southerly and south-easterly wind conditions. Central Bay shows extremely localized impacts to wave height, with much of the coastal area of this subregion being most disposed to wind waves from shore-normal directions.

3.2.3. Effect of Sea Level Rise on Wave Heights

To explore the impacts of SLR on 21st Century extreme wave heights, the fully coupled nonstationary wave-flow model (see the supporting information 1.1) was run over 2.2 days (over two tidal cycles) during a high-wind event (storm event) identified from the wave-screening process. For the storm-event simulation, the wave model included an additional wave grid offshore the Golden Gate, extending 10 km into the Pacific and 18 km north and south along the coast, in order to capture the propagation of deepwater waves through the Golden Gate. Return periods for wave heights were calculated by fitting generalized Pareto distributions to extreme H_s extracted for each basin from the wave-screening process. A 100 year event was then identified across the Bay to describe a region-wide 21st Century storm event.

The coupled model was run using the downscaled winds for the identified event. Wave spectra for the offshore wave-grid boundaries were extracted from available simulations of GFDL-ESM2M-derived waves for the Eastern Pacific [*Erikson et al.*, 2015] for the same time period. Thus, the influence of swell for the storm event is included. Offshore flow-grid boundaries were forced by 12 tidal constituents (see the supporting

Differences in H_s during 100-year storm with 1.0 m SLR

Figure 7. Maximum differences in H_s between a 100 year storm event with current water levels and with 1.0 m SLR.

information) as time-varying water levels for an idealized high spring tide [*Egbert et al.*, 1994; *Egbert and Erofeeva*, 2002; *National Oceanic and Atmospheric Administration (NOAA)*, 2016b]. Whereas storms occur independently of tides, a hypothetical worst-case scenario was assumed by synchronizing the wind and offshore-wave data to a high spring tide [*NOAA*, 2016b]. The same storm simulation was again run with 1.0 m static sea level rise added to the time-varying water levels, illustrating the effects of plausible sea level rise by 2100 [*Vermeer and Rahmstorf*, 2009; *National Research Council*, 2012]. Maximum storm period H_s was differenced between the 1.0 m SLR and present-day water level scenarios (Figure 7) to assess the effects of SLR on waves within the Bay.

During the storm event, the highest wave heights occurred in the deeper portions of Central Bay and South Bay (not shown). In the interior of Central Bay and the deeper portions of northern South Bay, maximum H_s during the event was much larger (over 3 m higher in the middle of Central Bay open to deep-water waves propagating through Golden Gate) than the maximum wave height identified through wave screening, owing to the inclusion of storm-related swell. However, with 1.0 m SLR, changes in H_s in these same regions were less than 0.15 m. Conversely, differences in H_s were larger within the nearshore and coastal sections throughout the Bay, predominantly beyond the influence of swell (Figure 7). These sections included the expansive shallow regions of Central and North Bay, sheltered from swell approaching from Golden Gate, but also the nearshore fringes throughout South Bay and North Bay. The largest changes (greater than 0.4 m) were within Central and North Bay, while widespread nearshore sections of South, Central, and North Bays showed differences in H_s greater than 0.25 m. Changes in Suisun Bay remained lower than elsewhere in the Bay. An additional 66 km^2 of coastal terrain were flooded throughout the Bay during this event with 1.0 m SLR than with present-day water levels.

4. Results and Discussion

4.1. Wind Projections for the 21st Century

Twenty-first century subdaily constructed wind fields showed good agreement with MACA-GFDL variation at key stations. Comparing 5 year averages of temporally downscaled and MACA-GFDL wind speeds for the 21st century projection period (Figure 8), temporally downscaled winds followed long-term changes in mean wind speed reflected in MACA-GFDL. As MACA-GFDL data represent daily averages, and subdaily wind vector components are quantile-corrected for MACA-GFDL bias and downscaled to 3-hourly time steps, a direct one-to-one relationship is not expected. Instead, long-term changes and variation are reflected in terms of changes in mean wind speed magnitude (S). Five-year averages of wind speed at SFO show the greatest correlation to MACA-GFDL ($r^2 = 0.79$, P value < 0.05), while winds at OAK displayed the smallest correlation ($r^2 = 0.62$, P value < 0.05). Inspections of maximum and extreme subdaily wind speeds in the temporally downscaled data showed a wide range of station behavior, as SFO and SJC showed fairly uniform and recurrent maximum projected subdaily wind speeds (~31 m/s), whereas TRAV displayed decadal variation in projected subdaily extreme wind speeds consistent with MACA-GFDL decadal variation at the location (not shown). Projected subdaily wind speed maxima across all key stations show little change at each station
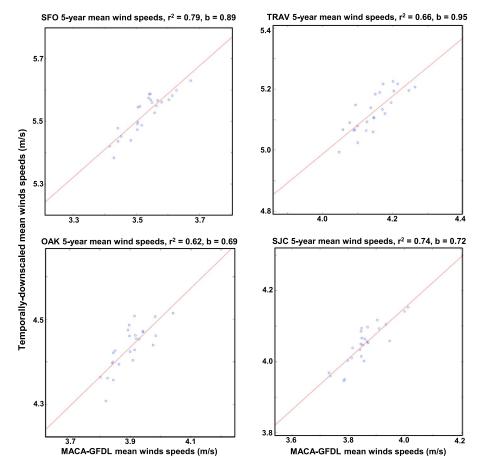
Figure 8. Projected (2014–2100) 5 year mean wind speeds for temporally downscaled and daily mean MACA-GFDL wind data at key stations.

from historical records. GFDL-ESM2M 3 h data (for the single Bay grid point) also show a negligible change in extreme subdaily wind speeds.

Looking at historical baseline over-water winds (1975–2004; Figure 9a and Table 2), the absolute highest speeds (S) are 41 m/s and 37 m/s in North Bay and Central Bay (respectively), and South Bay speeds reach 24 m/s (not shown). Upper quantile S (95th–99.9th quantiles) drop near or below 20 m/s for all subregions. South Bay holds the strongest wind speeds for all upper quantiles except the absolute maximum (not shown). Spatially, the lowest wind speeds are exhibited in the far southern reaches of the Bay, whereas the highest speeds are shown in the center portion of South Bay and the western portions of San Pablo Bay. High-wind events occurred both individually and as groups (e.g., consecutive days with upper quantile wind speeds).

Maximum over-water wind speeds for the entire 21st century projection period reach 34 m/s and 39 m/s in North and Central Bay, respectively, while maximum speeds reached 25 m/s in South Bay (not shown). Projections show a small increase in all upper quantile speeds (95th–99.9th quantiles) in North Bay for all 21st century periods (Table 2). The 98th percentile winds ($S98$) are shown as an example in Figure 9 and are representative of changes in other upper quantiles. Increases are greatest in western San Pablo Bay extending into Carquinez Strait. Central and South Bay exhibit mixed changes for wind speed. Upper quantile wind speeds in Central Bay show little change for most of the projection period, but decreases of ~2% are seen by the end of the Century. Across South Bay, wind speeds show small (±1%) variability through the projection period, but little cumulative change by the end of the Century. However, the far South Bay region displays different behavior than the rest of the basin with up to 3% decreases in upper quantile wind speeds by 2100 (Figure 9d).

In the entire 21st century downscaled projection series, 17 separate instances of winds exceed over-water benchmark values. Values are temporally grouped (occurring multiple times within four separate days),
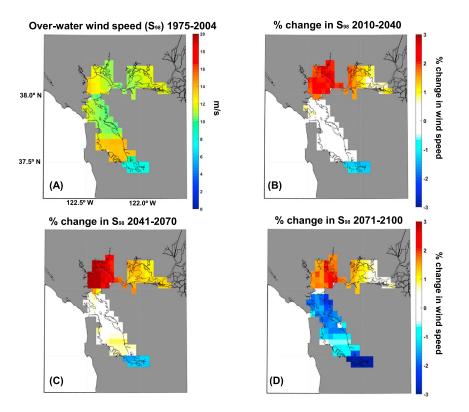
Figure 9. Projected % changes in extreme (98th quantile, S_{98}) over-water wind speeds. (a) Extreme wind speeds (S_{98}) for the time-slice representing the present climate (1975–2004). Changes in S_{98} for projected time periods (b) 2010–2040, (c) 2041–2070, and (d) 2071–2100, relative to the present time-slice.

much higher than benchmarks (~50 m/s), and the grid locations of the occurrences indicate similar numerical artifacts as seen in hindcast reconstructions. North Bay has the greatest number of exceedances (9), with the majority of the high-wind occurrences located on the far western side of San Pablo Bay. Originating MACA-GFDL wind fields for these occurrences show larger northwesterly wind speeds in this location than compared to elsewhere in the Bay. South Bay has only two instances of exceedance, and in each, the same grid points depict disproportionately high winds compared to adjacent grid points. As with historical reconstructions, these projection days are flagged and omitted from the analysis.

4.2. Wave Projections for the 21st Century

Projections of 21st century wave heights using the wave-screening method show wave patterns consistent with seasonal and episodic wind flow arrangements. Summer patterns show lower wave heights throughout the Bay, with the largest waves in those patterns in South Bay, Central Bay, and near straits: areas with the greatest fetch from onshore flow or in topographically constricted locations. The largest wave heights within the projection series are seen in fall and winter, with the greatest H_s in Central Bay. Wave heights peak in

Table 2. Extreme Over-Water Wind Speeds (S) (Maximum Within Each Subregion)

99.9th/99th/98th/95th Percentile Maximum S (m/s) With 95% Confidence Interval	South Bay	Central Bay	North Bay
Historical (1975–2004)	21.72 (21.56–21.88)	18.55 (18.34–18.80)	19.93 (19.61–20.24)
	16.24 (16.11–16.38)	14.41 (14.32–14.50)	15.19 (15.03–15.35)
	14.19 (14.11–14.27)	12.83 (12.71–12.95)	13.51 (13.41–13.60)
	12.26 (12.12–12.37)	11.03 (10.97–11.09)	11.31 (11.24–11.38)
Projected (2010–2100)	21.60 (21.50–21.69)	18.43 (18.25–18.58)	21.35 (21.05–21.70)
	16.14 (16.04–16.23)	14.34 (14.30–14.39)	15.49 (15.40–15.58)
	14.12 (14.08–14.17)	12.78 (12.71–12.84)	13.72 (13.66–13.79)
	12.16 (12.10–12.21)	10.97 (10.93–11.00)	11.50 (11.46–11.54)

Table 3. Extreme Bay Wave Heights (H_s)-Maximum Within Each Geographic Basin

99.9th/99th/98th/95th Percentile Local Maximum H_s (m) With 95% Confidence Intervals	South Bay	Central Bay	North Bay
Historical (1975–2004)	1.50 (1.43–1.46)	1.93 (1.63–1.98)	1.38 (1.28–1.58)
	1.30 (1.28–1.32)	1.25 (1.24–1.26)	1.11 (1.09–1.14)
	1.16 (1.15–1.18)	1.12 (1.11–1.14)	1.00 (0.98–1.11)
	1.05 (1.03–1.07)	0.96 (0.94–0.97)	0.86 (0.85–0.88)
Projected (2010–2100)	1.46 (1.45–1.47)	1.66 (1.54–1.91)	1.38 (1.33–1.49)
	1.31 (1.30–1.32)	1.25 (1.24–1.26)	1.12 (1.11–1.14)
	1.17 (1.16–1.18)	1.12 (1.11–1.13)	1.03 (1.02–1.04)
	1.04 (1.02–1.05)	0.95 (0.95–0.96)	0.88 (0.87–0.88)

areas where the Bay narrows, such as the southern end of Central Bay and where Central Bay transitions to North Bay, and in the large interior fetch of South Bay. Outside these recurring high-wave instances, winter patterns are generally calm with prevalent low waves (less than 0.5 m in protected embayments). Both single-day and multiday high-wave episodes are observed within the projection period.

Local maxima of H_s at upper and extreme quantiles (95th–100th quantiles) were identified within each subregion. A spatial-average of extreme H_s, representative of conditions across the subregion, was also determined and summarized in Tables 3 and 4. Error at the 95% confidence interval was determined via the bootstrap method. The 98th percentile wave heights (H_{s98}) are shown as an example and representative of changes in other upper quantiles (Figure 10).

Looking at the hindcast wave-screening of (1975–2004) of H_s, upper quantile H_s (95th–99.9th quantiles) are below 1.5 m for all subregions except Central Bay where historical $H_{s99.9}$ is 1.9 m (Figure 10 and Tables 3 and 4). The highest H_s for all upper quantiles are located in Central and South Bays. Spatially, the lowest H_s are exhibited in the nearshore reaches of each subregion, whereas the highest H_s are shown in the deep channels of Central and South Bays, along the area of largest fetch, and in straits and narrows where wind speeds also increased (Figures 9 and 10). Longest wave periods (T_p) are seen in similar areas and greatest fetch and in terrain-restricted narrows (Figure 11).

Projections from 21st century simulation results show an increase in all upper quantile local maxima and regional average H_s in North Bay (Figures 10b–10d and Tables 3 and 4). Increases in H_s are greatest in southern San Pablo Bay, connecting to Central Bay, and Carquinez Strait. North Bay T_p likewise shows similar and consistent increases (Figure 11). While some localized increases in H_{s98} are depicted midcentury along the eastern boundaries of the region, cumulative changes by end century for both local H_s and subregional H_s maximums show downward changes. South Bay shows increases in local maximum H_s through the end of the century but decreases in spatially averaged conditions. H_s spatial changes show increases across the subregion in midcentury but remain unchanged or show slight decreases in the beginning and ending periods (Figures 10b–10d). The far southern region of South Bay displays mixed changes throughout the projection period, with small localized increases along the southern shores at beginning and midcentury, but decreases toward end-century (Figure 10). Changes in T_p remain mixed to neutral for Central and much of South Bay, while the far southern region of South Bay displays decreases in T_p for the entire period (Figure 11). Specific occurrences of extreme wave events were correlated between subregions; however, the severity

Table 4. Extreme Bay Wave Heights (H_s)-Spatial-Average Within Each Geographic Basin

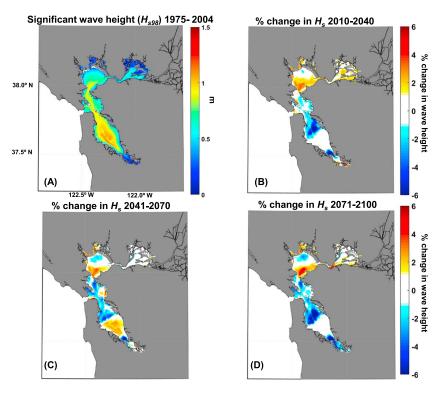| 99.9th/99th/98th/95th Percentile Spatial-Average H_s (m) With 95% Confidence Intervals	South Bay	Central Bay	North Bay
Historical (1975–2004)	0.68 (0.68–0.69)	1.15 (1.07–1.18)	0.59 (0.58–0.62)
	0.66 (0.65–0.67)	0.77 (0.74–0.80)	0.48 (0.47–0.49)
	0.65 (0.64–0.66)	0.66 (0.65–0.68)	0.46 (0.45–0.47)
	0.57 (0.56–0.58)	0.59 (0.58–0.60)	0.44 (0.43–0.44)
Projected (2010–2100)	0.67 (0.66–0.67)	1.05 (1.04–1.12)	0.60 (0.58–0.61)
	0.64 (0.64–0.64)	0.76 (0.74–0.78)	0.50 (0.49–0.51)
	0.62 (0.61–0.62)	0.65 (0.64–0.66)	0.47 (0.46–0.47)
	0.55 (0.54–0.56)	0.59 (0.58–0.59)	0.44 (0.43–0.44)

Figure 10. Projected changes in storm-related extreme wave heights (98th quantile, H_{S98}). (a) Extreme significant wave heights (H_{S98}, m) for the time-slice representing the present climate (1975–2004). Changes in H_{S98} for projected time period s (b) 2010–2040, (c) 2041–2070, and (d) 2071–2100, relative to the present time-slice.

of the events differed. For example, a 99.9th quantile event in one subregion occurred as a 98th or 95th quantile event in other subregions. No single extreme wave event occurred at the same quantile across the Bay's subregions.

4.3. Discussion

While the process of identifying appropriate analogues and applying its data to increase resolution is an imperfect process, the results are improved when originating model output captures large-scale patterns and behavior well. MACA-GFDL data adequately capture the bulk of daily wind behavior for SFO, OAK, and TRAV, but wind speeds at SJC are overpredicted. The MACA-GFDL daily data do not capture light, calm periods or vector component extremes in the far South Bay as well, and the effect is ultimately translated to downscaled output. While deviations of extreme wind speed values in hindcast winds up to 9 m/s were observed in the meridional component of hindcast reconstructions at TRAV, OAK, and SJC, wave sensitivity analysis showed that deviations in extreme values are not in the direction of importance for wave generation and local flooding at TRAV and OAK. Therefore, the deviations in wind extremes minimally impact extreme event-based flooding projections for which these data will be used. However, in the far South Bay, MACA-GFDL data and reconstructions did not adequately resolve vector component distributions or extremes. In South Bay therefore wave projections made using temporally downscaled MACA-GFDL winds may underestimate potential wave impacts in the area, as well as any associated flooding in follow-on work. Deviations in reconstructed extreme wind speed values are likely due to the quantile correction method used; it was a direct arithmetic correction, not accounting for future changes in distribution. Applying quantile corrections from hindcast data accounts for known bias in model output. However, as future atmospheric conditions may alter, wind distributions may change, as well as bias. Improvements to the methodology presented herein may be achieved through quantile-correction techniques that account for future changes in distribution [*Vrac et al.*, 2012], and are left for future work.

Similarly, future projections do not always have a good historical analogue, as the future may not mimic observed patterns. In some projections, particularly during low-speed calm periods, a good "match" was
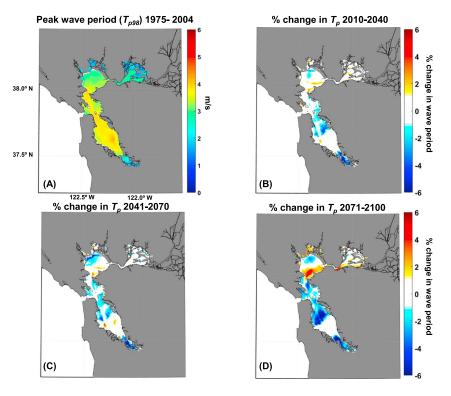
Figure 11. Same as Figure 10 for peak wave periods (T) associated with extreme wave heights. (a) Storm-related wave periods (T_{p98}, s) for the time-slice representing the present climate (1975–2004). Changes in T_{p98} for projected time periods (b) 2010–2040, (c) 2041–2070, and (d) 2071–2100, relative to the present time-slice.

harder to identify and error was much higher. This is good to keep in mind for applications using the entirety of the data output, but as the interest of this study is storm-related extreme wind speed events, this was not a significant detractor.

For a more complete characterization of 21st Century extreme wind projections, multiple GCM-derived MACA data sets can be downscaled in a similar manner, for a multimodel investigation of wind change statistics. Such multimodel comparisons may yield changes not apparent in the temporally downscaled MACA-GFDL data. Other GCMs and derived MACA data sets may also better represent climatic changes in the study area. However, an extensive analysis of a series of GCMs is beyond the scope of this study, as the focus in more of the development of the technique, rather than assuring a full range of possible wind forcing scenarios. Similarly, MACA is not the single source of spatially downscaled GCM data available for the study region. At the time of this work, MACA data sets were the only known source of wind data at sufficient spatial resolution within the San Francisco Bay for wave modeling. Comparisons to other downscaled data sets have not been made.

Reconstructed hindcasts of extreme winds within Central Bay are underestimated. Considering that station reconstructions at OAK were represented well (especially in dominant eastward directions), hindcasts of the subregion's interior show lower eastward wind speeds for many upper quantiles. Contrary to similar comparisons in South Bay and North Bay, OAK may not be the most accurate representation of wind variation through Central Bay. OAK is set back from the interior of the region, away from where winds enter through Golden Gate or terrain may enhance wind speeds. Therefore, OAK may miss important wind variation observed within the interior and straits of this subregion. However, as there are no other observation stations with as long and detailed wind records, this is the best option to approximate Central Bay conditions for this study.

Instances of overwater wind speeds exceeding study thresholds were primarily observed on the far western side of San Pablo Bay (bordering marsh/wetlands, near foothills of Marin County) and in 6-7 grid points bordering South Bay. These instances of exceedance are likely numeric artifacts stemming from several sources.

First, as MACA-GFDL winds showed consistently higher daily average wind speeds near the foothills of Marin County than at TRAV, daily correctional factors determined at TRAV (east side of North Bay subregion) may not have accounted for wind adjustments in the far west side of the subregion as well as near the observation station. Terrain varies in height and orientation in the two areas and thus may play a larger role than anticipated in both direction and speed variation between the areas of this subregion. Additionally, originating MACA-GFDL daily average wind speeds in portions of San Pablo Bay and South Bay may be too high and thus accentuated during the temporal downscaling process. Locations of these instances coincided with wind speeds that were flagged as part of the hindcast reconstruction, further suggesting these instances as persistent numeric artifacts. Originating wind data may also have occasional erroneously high values at specific grid points. During both the hindcast and 21st century projection temporal downscaling processing, specific South Bay grid points showed consistent exceedance of thresholds by almost 2 orders of magnitude (well outside 3 standard deviations from subregion station's mean wind speed), far larger than expected given neighboring values and station reconstructions. These specific grid points were replaced with adjacent values, which better displayed subregional behavior.

The temporal-downscaling process provided the necessary subdaily resolution for determination of wind-generated storm waves. Daily mean wind speeds in MACA-GFDL were half the maximum subdaily wind speeds in some upper-quantile events. Such large disparities in wind speed have a significant impact on resulting wave heights in the Bay. For instance, using a simple analytical wave height estimation [*Coastal Engineering Research Center*, 1984] in the South Bay adjacent to SFO (with consistent westerly winds), MACA-GFDL's extreme daily wind speed of 10 m/s (Figure 3) yields a wave height estimate of 0.62 m in the basin west of the station. However, historical observations and temporally downscaled reconstructions show extreme westerly winds can reach speeds up to 20 m/s, resulting in wave heights of 1.2 m. Up to 50% of the significant wave height is missed if subdaily variation is not used.

Overall, SWAN hindcasts corroborate with measurements and anecdotal reports of Bay wave heights and patterns. Maximum waves are observed along areas of the greatest fetch in deeper straits and in narrows where enhanced wind may drive localized wave generation. As many of the upper quantile wave heights were located in the deeper channel areas of Central Bay to South Bay, this may also suggest the relative importance of southerly winds for extreme wave generation within the Bay, given the similarity to results from steady state determination tests (see section 2.4). This scenario is also consistent with expected wave growth in relation to depth changes proceeding north along axis from South Bay to Central Bay. While occurrences of upper quantile (95th–99.9th) wave height extremes were higher in large fetch areas and near straits/narrows (such as illustrated in North Bay), region-wide conditions were higher in Central Bay. The SWAN model used to determine projected wave heights does not account for currents or changes in water levels and therefore does not assess the spatial variability of wave heights due to wave-current interaction and depth changes. However, it simulates ~85% of wave energy (as shown in section 2.4) in a computationally efficient method. Overall, SWAN-modeled wave heights adequately represent the wind-wave climate of San Francisco Bay, particularly during extreme conditions, as this wind-based wave-screening is sufficient to identify storm periods and potential wave heights. Identified wave heights using this method are likely biased low as it does not account for at least 15% of H_s present when considering wave-current interaction. Given this shortfall in modeled wave height, hindcast maximum wave heights could reflect H_s of over 2.2 m and potential 21st century H_s could reach up to 2.0 m in Central Bay, excluding the effects of ocean swell penetrating through the Golden Gate.

Additionally, this paper is not meant to authoritatively speak to historical and projected wave height distributions but to provide methods to screen for major storm events and evaluate likely changes in the 21st century wave climate. Identified storm events will be modeled with a high-resolution two-way coupled FLOW-WAVE model including tides, atmospheric surface pressure, fluvial discharge estimates, space, and time-varying high-resolution winds presented in this study, and potential sea level rise.

While there is little change in the intensity of Bay area wind speeds or height of maximum storm waves in this combined approach, using the projected downscaled winds is still advantageous over existing historically based wind fields and wave model data. First, existing wind fields depicting historical conditions do not have the fine-scale spatial variation and resolution of these data sets. The resolutions offered by the time-downscaled winds and resultant wind-wave projections are ideal for multiple follow-on projects and

investigations. Also, these projections are consistent with GFDL and MACA-GFDL decadal and intradecadal trends and thus are ideal for climate-related work. As illustrated by the wave sensitivity portion of this paper, wind speed alone is not the sole determination of wave height, as direction is also an important aspect of wave generation. Changes in wind direction can alter areas of resultant maximum wave energy and can also alter how wind may interplay with topography. While not addressed in this paper, overwater changes in wind direction may also yield significant changes to surface currents and further alter wave heights. Thus, any changes in storm-related wind direction may alter wave height and any associated on-shore flooding. Fully coupled nonstationary flow-wave simulations for several extreme events identified from the wave screening, ideally representing the variety of storm-wind directions affecting the diverse coastline within the Bay, need to be run for a complete look into the impact of direction on wave height, including wave-current interaction, and flood hazards.

Sensitivity tests showed that the influence of SLR on wave growth was most prominent in shallow areas along the Bay shoreline and across tidal flats. Excluding the contributions of open-ocean swell and accounting for locally generated wind waves only, the highest wave heights within the deeper portions of the Bay show little change with 1.0 m SLR. Even with the addition of more extreme SLR projections, the rise in water level in relation to the deep channels is small ($\sim <5\%$), and significant changes in wave height would not be expected due to water level. Based on sensitivity tests, modified circulation driven by the rise in water level may force H_s changes, but further study is needed to determine the extent of those circulation and wave-current interaction changes. Ideally, simulations for a range of SLR, both including and neglecting wave-current interaction, are necessary to characterize how H_s in the deeper portions may change over the next century. However, wave heights along the nearshore and coastal areas, where water level has a greater influence on wave growth, show significant increases with a 1.0 m rise in sea level, with H_s almost 0.5 m higher in nearshore sections of Central and North Bay. The relative increase in shallow-water H_s does not exceed the maximum H_s in deep channels in this 1.0 m SLR example. However, in higher SLR scenarios and lower intensity storms, the relative increase in shallow-water H_s may approach the wave height in deeper portions. During such instances, wave-screening results may not yield an accurate spatial characterization of maximum wave height, though the occurrence of the extreme event (Bay-wide maximum H_s) would still be apparent. Consequently, more information than the wave-screening H_s time series is needed to resolve extreme storm event return periods (section 2.4) and identify representative 21st century storms for the purpose of coastal flood projections. Most importantly, however, with increasing SLR, wave heights escalate the most in the shallow stretches adjacent to urban and residential areas. Thus, SLR contributes to flood hazards not only by increasing water levels but also via greater wave growth potential in shallow regions along the Bay.

5. Conclusions

In San Francisco Bay, neither coarse Global Climate Model data nor historical observations provide enough spatial (~200 km) or temporal resolution (approximately daily) to accurately compute the generation of local wind waves for studies of flood hazards. In order to provide input for coastal flood hazard modeling, downscaled wind at timescales small enough to resolve local wave generation during the peaks of extreme storm events is required. In this study, extensive historical wind observations at representative stations throughout San Francisco Bay were used to temporally downscale a high-resolution statistically downscaled climate model and generate a data set of near surface wind fields (resolution 4 km) at 3 h time steps for historical (1975–2004) and 21st century (2010–2100) projections. Hindcasts accurately recreate long-term wind conditions and extreme events at key observation stations throughout the Bay.

Wave simulations using a single, curvilinear SWAN model covering the entire Bay were run for hindcast and 21st century projection periods. Simulations were run using daily time steps and the daily maximum wind conditions determined from 3-hourly downscaled time series each day, as a computationally efficient method for identifying extreme events over long time periods. Wave model skill is good, as shown by validation runs with a coupled hydrodynamic model compared to observations.

Twenty-first century projections show little change in the magnitude of extreme wind speeds and locally generated waves. However, this depiction neglects the contribution of SLR on wave height in the shallower portions of the Bay. A characterization of coincident wind and wave direction throughout the period will give

a more complete understanding of possible changes in storm conditions. Further investigation into the spatial variance in projected trends of extreme wind and wave conditions may yield more insight into local storm-related impacts. However, the use of these downscaled winds and efficient screening for high-wave events allows rapid identification of 21st century storms and the means by which to simulate detailed wind-wave generation in more complex storm-event simulations. This work will aid follow-on investigations into the regionalized impacts of wave-current interaction and more accurate event-based modeling for future coastal flooding assessments using CoSMoS.

References

Abatzoglou, J. T. (2013), Development of gridded surface meteorological data for ecological applications and modelling, *Int. J. Climatol.*, *33*, 121–131, doi:10.1002/joc.3413.

Abatzoglou, J. T., and T. J. Brown (2012), A comparison of statistical downscaling methods suited for wildfire applications, *Int. J. Climatol.*, *32*, 772–780, doi:10.1002/joc.2312.

Allan, J. C., P. D. Komar, and P. Ruggiero (2011), Storm surge magnitude and frequency on the central Oregon coast, Proc. Solutions to Coastal Disasters Conf., Amer. Soc. Civil Engrs., Anchorage, Alaska: 209-220.

Alves, J. H. G. M., A. Chawla, H. L. Tolman, D. J. Schwab, G. Lang, and G. Mann (2011), The Great Lakes wave model at NOAA/NCEP: challenges and future developments, Conf. Proc. 12th Intl. Wrkshp Wave Hindcasting and Forecasting, Kohala Coast, Hawai'i.

Barnard, P. L., D. M. Hanes, D. M. Rubin, and R. G. Kvitek (2006), Giant sand waves at the mouth of San Francisco Bay, *Eos. Trans. AGU*, *87*(29), 285–289.

Barnard, P. L., and R. G. Kvitek (2010), Anthropogenic influence on recent bathymetric change in west-central San Francisco Bay, *San Franc. Estuary Watershed Sci.*, *8*(3), 13.

Barnard, P. L., D. H. Schoellhamer, B. E. Jaffe, and L. J. McKee (2013), Sediment transport in the San Francisco Bay Coastal System: An overview, *Mar. Geol.*, *345*, 3–17, doi:10.1016/j.margeo.2013.04.005.

Barnard, P. L., O. van Maarten, L. H. Erikson, J. Eshleman, C. Hapke, P. Ruggiero, P. Adams, and A. Foxgrover (2014), Development of the Coastal Storm Modeling System (CoSMoS) for predicting the impact of storms on high-energy, active-margin coasts, *Nat. Hazards*, *74*(2), 1095–1125, doi:10.1007/s11069-014-1236-y.

Battjes, J. A., and J. P. F. M. Janssen (1978), Energy loss and set-up due to breaking of random waves, Proc. 16th Intl. Conf. on Coastal Eng., Amer. Soc. Civil Engrs, 569–587.

Brekke, L., B. Thrasher, E. Maurer, and T. Pruitt (2013), Downscaled CMIP3 and CMIP5 climate projections; Release of downscaled CMIP5 climate projections, comparison with preceding information and summary of user needs, May (report). [Retrieved from http://gdo-dcp.ucllnl.org/downscaled_cmip_projections/on 01 July 2013.]

Booij, N., R. C. Ris, and L. H. Holthuijsen (1999), A third-generation wave model for coastal regions Model description and validation, *J. Geophys. Res.*, *104*, 7649–7666.

Cayan, D. R., P. D. Bromirski, K. Hayhoe, M. Tyree, M. D. Dettinger, and R. E. Flick (2008), Climate change projections of sea level extremes along the California coast, *Clim. Change*, *87*(Suppl.1), 57–73.

Cloern, J. E., et al. (2011), Projected evolution of California's San Francisco Bay-Delta-River system in a century of climate change, *PLoS One*, *6*(9), 13.

Coastal Engineering Research Center (1984), Shore Protection Manual, U.S. Army Corps of Engineers, Waterways Experiment Station, Vicksburg Mississippi.

Conner, K. L., D. R. Kerper, L. R. Winter, C. L. May, and K. Schaefer (2011), Coastal flood hazards in San Francisco Bay–A detailed look at variable local flood responses, *Solutions Coast. Disasters*, 448–460, doi:10.1061/41185(417)40.

Dorman, C. E., and C. D. Winant (1995), Buoy observations of the atmosphere along the west coast of the United States, 1981–1990, *J. Geophys. Res.*, *100*(C8), 16,029–16,044, doi:10.1029/95JC00964.

Dunne, J. P., et al. (2012), GFDL's ESM2 global coupled climate–carbon earth system models, Part I: physical formulation and baseline simulation characteristics, *J. Clim.*, *25*, 6646–6665, doi:10.1175/JCLI-D-11-00560.1.

Egbert, G. D., A. F. Bennett, and M. G. G. Foreman (1994), TOPEX/POSEIDON tides estimated using a global inverse model, *J. Geophys. Res.*, *99*, 24821–24852, doi:10.1029/94JC01894.

Egbert, G., and S. Erofeeva (2002), Efficient inverse modeling of barotropic ocean tides, *J. Atmos. Ocean. Technol.*, *19*, 183–204.

Elias, E. P. L., and J. E. Hansen (2012), Understanding processes controlling sediment transports at the mouth of a highly energetic inlet system (San Francisco Bay, CA), *Mar. Geol.*, *345*, 207–220, doi:10.1016/j.margeo.2012.07.003.

Environmental Modeling Center (2003), The GFS atmospheric model, NCEP Office Note 442, Global Climate and Weather Modeling Branch, EMC, Camp Springs, Maryland.

Erikson, L. H., S. A. Wright, E. Elias, D. M. Hanes, D. H. Schoellhamer, and J. Largier (2013), The use of modeling and suspended sediment concentration measurements for quantifying net suspended sediment transport through a large tidally dominated inlet, *Mar. Geol.*, *345*, 96–112, doi:10.1016/j.margeo.2013.06.001.

Erikson, L. H., C. A. Hegermiller, P. L. Barnard, P. Ruggiero, and M. van Ormondt (2015), Projected wave conditions in the Eastern North Pacific under the influence of two CMIP5 climate scenarios, *Ocean Model.*, *96*, 171–185, doi:10.1016/j.ocemod.2015.07.004.

Ganju, N. K., B. E. Jaffe, and D. H. Schoellhamer (2011), Discontinuous hindcast simulations of estuarine bathymetric change: A case study from Suisun Bay, California, *Estuar. Coast. Shelf Sci.*, *93*, 142–150.

Guza, R. T., and E. B. Thornton (1981), Wave set-up on a natural beach, *J. Geophys. Res.*, *86*, 4133–4137.

Hall, A., et al. (2012), Mid-century warming in the Los Angeles region—Part I of the "Climate change in the Los Angeles region" project, UCLA: Institute of the Environment and Sustainability. [Retrieved from: http://escholarship.org/uc/item/6v88k76b]

Hanes, D. M., K. Ward, and L. H. Erikson (2011), Waves and tides responsible for the intermittent closure of the entrance of a small, sheltered tidal wetland at San Francisco Ca, *Cont. Shelf Res.*, *31*, 1682–1687.

Hasselmann, K., et al. (1973), Measurements of wind-wave growth and swell decay during the Joint North Sea Wave Project (JONSWAP), *Ergnzungsheft zur Deutschen Hydrographischen Zeitschrift Reihe*, *8*(12), 95.

Hidalgo, H. G., M. D. Dettinger, and D. R. Cayan (2008), Downscaling with constructed analogues: Daily precipitation and temperature fields over the United States, California Energy Commission, PIER Energy-Related Environmental Research, CEC-500-2007-123.

Joyner, T. A (2013), Optimizing peak gust and maximum sustained wind speed estimates for mid-latitude wave cyclones, PhD Dissertation, Louisiana State University. [Retrieved from http://sites01.lsu.edu/wp/graduateschool/thesis-and-dissertation-library/ (etd-04052013-150210).]

Kanamitsu, M., and H. Kanamaru (2007a), 57-year California reanalysis downscaling at 10 km (CaRD10): Part 1. System detail and validation with observations, *J. Clim.*, *20*, 5527–5552.

Kanamitsu, M., and H. Kanamaru (2007b), 57-year California reanalysis downscaling at 10 km (CaRD10): Part 2. Comparison with North American Regional Reanalysis, *J. Clim.*, *20*, 5553–5571.

Kerper, D., J. A. Zyserman, T. Shen, and C. M. Appendini (2011), Regional coastal hazard modeling study for North and Central San Francisco Bay, DHI Water and Environment, Inc., Final Draft Report, October.

Lacy, J., and D. Hoover (2011), Wave exposure of Corte Madera Marsh, Marin County, California—A field investigation, *U.S. Geol. Surv. Open File Rep.*, *2011-1183*. [Available at http://pubs.usgs.gov/of/2011/1183/]

Lacy, J., S. Gladding, A. Brand, A. Collignon, and M. Stacey (2014), Lateral baroclinic forcing enhances sediment transport from shallows to channel in an estuary, *Estuaries Coasts*, *37*(5), 1058–1077, doi:10.1007/s12237-013-9748-3.

Ludwig, F. L., J. M. Livingston, and R. M. Endlich (1991), Use of mass conservation and critical dividing streamline concepts for efficient objective analysis of winds in complex terrain, *J. Appl. Meteorol.*, *30*(11), 1490–1499.

Marine Exchange of the San Francisco Bay Region (2016), Weather in the San Francisco Bay. [Retrieved from http://www.sfmx.org/support/amsc/on 01 Nov 2013.]

Maurer, E. P., L. Brekke, T. Pruitt, and P. B. Duffy (2007), Fine-resolution climate projections enhance regional climate change impact studies, *Eos. Trans. AGU*, *88*(47), 504.

National Climatic Data Center (NCDC) (2013), Storm events database, Strong/high marine and coastal wind and winter weather events in San Francisco region. [Retrieved from https://www.ncdc.noaa.gov/stormevents/ on 01 May 2013.]

National Oceanic and Atmospheric Administration (NOAA) (2016a), Severe weather data inventory, National Climatic Data Center. [Available at http://www.ncdc.noaa.gov/swdi/#TileSearch.]

National Oceanic and Atmospheric Administration (NOAA) (2016b), Tides & currents, Center for Operational Oceanographic Products and Services. [Available at http://tidesandcurrents.noaa.gov/.]

National Research Council (2012), Sea-level rise for the coasts of California, Oregon, and Washington: past, present, and future, Committee on Sea Level Rise in California, Oregon, and Washington, 260 pp., The National Academies Press, Washington.

Nicholls, R. J. (2004), Coastal flooding and wetland loss in the 21st century: Changes under the SRES climate and socio-economic scenarios, *Glob. Environ. Chang.*, *14*, 69–86, doi:10.1016/j.gloenvcha.2003.10.007.

Olabarrieta, M., J. C. Warner, and N. Kumar (2011), Wave-current interaction in Willapa Bay, *J. Geophys. Res.*, *116*, C12014, doi:10.1029/2011JC007387.

Olabarrieta, M., R. Geyer, and N. Kumar (2014), The role of morphology and wave-current interaction at tidal inlets: An idealized modeling analysis, *J. Geophys. Res. Oceans*, *119*, 8818–8837, doi:10.1002/2014JC010191.

Patton, C. (1956), *Climatology of Summer Fogs in the San Francisco Bay Area*, pp. 114–145, Univ. of California Press, Berkeley.

Pacific Climate Impacts Consortium, University of Victoria (2014), Statistically Downscaled Climate Scenarios, January (report). [Retrieved from http://tools.pacificclimate.org/dataportal/downscaled_gcms/map/on Sep 1, 2014.]

Putnam, J. A. (1947), Estimating storm-wave conditions in San Francisco Bay, *Trans. AGU*, *28*, 271–278.

Ris, R. C. (1997), Spectral modelling of wind waves in coastal areas, PhD Dissertation, Delft University of Technology, Communications on Hydraulic and Geotechnical Engineering, Report No. 97-4.

Ris, R. C., L. H. Holthuijsen, and N. Booij (1999), A third-generation wave model for coastal regions 2. Verification, *J. Geophys. Res.*, *104*, 7667–7681.

Rogers, W., J. Kaihatu, L. Hsu, R. Jensen, J. Dykes, and K. Holland (2007), Forecasting and hindcasting waves in the SWAN model in the Southern California Bight, *Coast. Eng.*, *54*, 1–15.

Ross, S. (2001), Synoptic and topographic forcing of microclimates across San Francisco Bay, Unpublished thesis dissertation, University of Delaware, Newark, Delaware.

Ryan, H., H. Gibbons, J. Hendley, and P. Stauffer (1999), El Niño sea-level rise wreaks havoc in California's San Francisco Bay Region, *U.S. Geol. Surv. Fact Sheet 175-99*. [Retrieved from http://pubs.usgs.gov/fs/1999/fs175-99/ on 01 March 2015.]

Solari, G. (1993), Gust buffeting I. Peak wind velocity and equivalent pressure, *J. Struct. Eng. Amer. Soc. Civ. Eng.*, *119*, 365–382.

Taylor, K. E., R. J. Stouffer, and G. A. Meehl (2012), An overview of CMIP5 and the experiment design, *Am. Meteorol. Soc.*, doi:10.1175/BAMS-D-11-00094.1.

Talke, S. A., and M. T. Stacey (2003), The influence of oceanic swell on flows over an estuarine intertidal mudflat in San Francisco Bay, *Estuar. Coast. Shelf Sci.*, *58*, 541–554.

Tyler, D. J., J. J. Danielson, J. C. Brock, A. C. Foxgrover, and P. L. Barnard (2014), Topobathymetric model of the San Francisco Bay area, California, Coastal National Elevation Database (CoNED) Applications Project. [Available at http://topotools.cr.usgs.gov/coned/sanfrancisco.php.]

Vermeer, M., and S. Rahmstorf (2009), Global sea level linked to global temperature, *Proc. Natl. Acad. Sci. Amer.*, *106*(51), 21527–21532, doi:10.1073/pnas.0907765106.

Vrac, M., P. Drobinski, A. Merlo, M. Herrman, C. Lavaysse, L. Li, and S. Somot (2012), Dynamical and statistical downscaling of the French Mediterranean climate: uncertainty assessment, *Nat. Hazards Earth Syst. Sci.*, *12*, 2769–2784, doi:10.5194/nhess-12-2769-2012.

van der Westhuysen, A. J., M. Zijlema, and J. A. Battjes (2007), Nonlinear saturation-based whitecapping dissipation in SWAN for deep and shallow water, *Coast. Eng.*, *54*, 151–170.

van Raalten, D., et al. (2009), San Francisco Bay: preparing for the next level, ARCADIS cooperative report. [Retrieved from http://www.bcdc.ca.gov/planning/climate_change/SFBay_preparing_%20for_the_next_Level.pdf on 01 March 2015.]